Molecular Therapy
Advances
Original Article

Efficacy of anti-VEGF single-chain variable fragment AAV-based gene therapy in a laser-induced choroidal neovascularisation mouse model

Ahmed Salman,[1] Helen Griffiths,[2] Kamaluddeen Garba,[2] Savannah A. Lynn,[2] Angela J. Cree,[2] Manon Szczepan,[7] Charnitkaur B. Jashal,[6] Rajanathan Chozhavel T M,[6] Poornima Rao,[6] Kush Modi,[6] Robert E. MacLaren,[1,4] Ho Ming Yuen,[5] and Andrew J. Lotery[2,3]

[1]Nuffield Department of Clinical Neurosciences, University of Oxford, Oxford, UK; [2]Clinical and Experimental Neurosciences, Faculty of Medicine, University of Southampton, Southampton, UK; [3]Southampton Eye Unit, Southampton General Hospital, Southampton, UK; [4]Oxford Eye Hospital, Oxford, UK; [5]School of Primary Care, Population Sciences and Medical Education, Faculty of Medicine, University of Southampton, Southampton, UK; [6]Intas Pharmaceuticals Ltd, Ahmadabad, India; [7]The Wellcome-Wolfson Institute for Experimental Medicine, School of Medicine, Dentistry & Biomedical Sciences, Queen's University Belfast, Belfast, Northern Ireland

Age-related macular degeneration (AMD) is a leading cause of vision loss in the elderly. Neovascular AMD (nAMD) is characterized by abnormal growth of new blood vessels from the choroid (choroidal neovascularization, CNV), with retinal pigment epithelium dysfunction leading to fluid leakage, bleeding, and central vision loss. nAMD is primarily driven by vascular endothelial growth factor (VEGF). Anti-VEGF therapies are widely used, with brolucizumab, a humanized monoclonal single-chain variable fragment (scFv) that inhibits VEGF, showing promise due to its high molar concentration and superior ability to dry the retina. However, concerns over retinal vasculitis have limited its clinical use. In this proof-of-principle study, we evaluated an AAV-delivered anti-VEGF scFv transgene derived from the brolucizumab sequence, packaged into two recombinant adeno-associated virus serotypes (rAAV6 and rAAV8), and delivered via subretinal injections in a laser-induced CNV mouse model. Leakage in 79 mice across seven groups was assessed by fundus fluorescein angiography. Compared with controls, AAV-treatment showed reduced leakage, particularly at week 9 (3.1% for rAAV6 and ∼10% for rAAV8 high doses), compared with controls (71.9%). Vector genomes were detectable by qPCR at 12 weeks, and electroretinography showed no obvious functional deficit. These findings support further evaluation of sustained AAV-mediated anti-VEGF delivery for nAMD.

INTRODUCTION

Age-related macular degeneration (AMD) is the leading cause of irreversible central vision loss in the elderly in developed countries with a prevalence of 8.7%.[1,2] It is assumed that about 10% of the population over 65 years and 25% over 75 years have been diagnosed with AMD.[3,4] Worldwide, it is estimated that the number of individuals with AMD will reach 288 million by 2040,[1] with the number of cases continuously increasing. Clinical manifestations range from asymptomatic early and intermediate stages, into significant vision loss in late or advanced AMD. The latter has two categories: neovascular (wet) and non-neovascular (dry).[5] Wet or neovascular AMD (nAMD) is characterized by atrophy and degeneration of the neuroretina, retinal pigment epithelial (RPE), and choriocapillaris.[5] Choroidal neovascularization (CNV) in the macula is the hallmark of nAMD,[6] with subretinal and intravitreal fluid, retinal, subretinal, and sub-RPE hemorrhage, lipid exudates, RPE detachment, and RPE tear also involved.[5,7]

Approximately 10% of early-stage AMD advances into a late stage,[8] influenced by the upregulation of the vascular endothelial growth factor (VEGF), which is the key mediator of AMD progression from early/intermediate to late-stage nAMD.[8] VEGF is a growth factor that stimulates the growth of blood vessels,[9] leading to the promotion of angiogenesis in the initial CNV, increasing vascular permeability and the appearance of new blood vessels that leak into the macula.[10,11] Dysfunction and degeneration of the RPE cells, which is essential for maintaining the health of the light-sensitive cells of the retina, the photoreceptors.[12]

Successful anti-VEGF treatment strategies in the past decades have met relative success in halting the progression of nAMD,[10,13–17] including anti-VEGF gene therapy approaches with ranibizumab[17,18] and bevacizumab,[19–21] further elucidating the importance of VEGF in the progression of the disease. brolucizumab is a recently approved anti-VEGF agent for nAMD.[22] Its arrival was highly anticipated in the ophthalmological community due to its longer duration of fluid control despite reduced dosing frequency compared with

Received 7 January 2026; accepted 6 May 2026;
https://doi.org/10.1016/j.omta.2026.201756.

Correspondence: Andrew J. Lotery, Clinical and Experimental Neurosciences, Faculty of Medicine, University of Southampton, Southampton, UK.
E-mail: a.j.lotery@soton.ac.uk

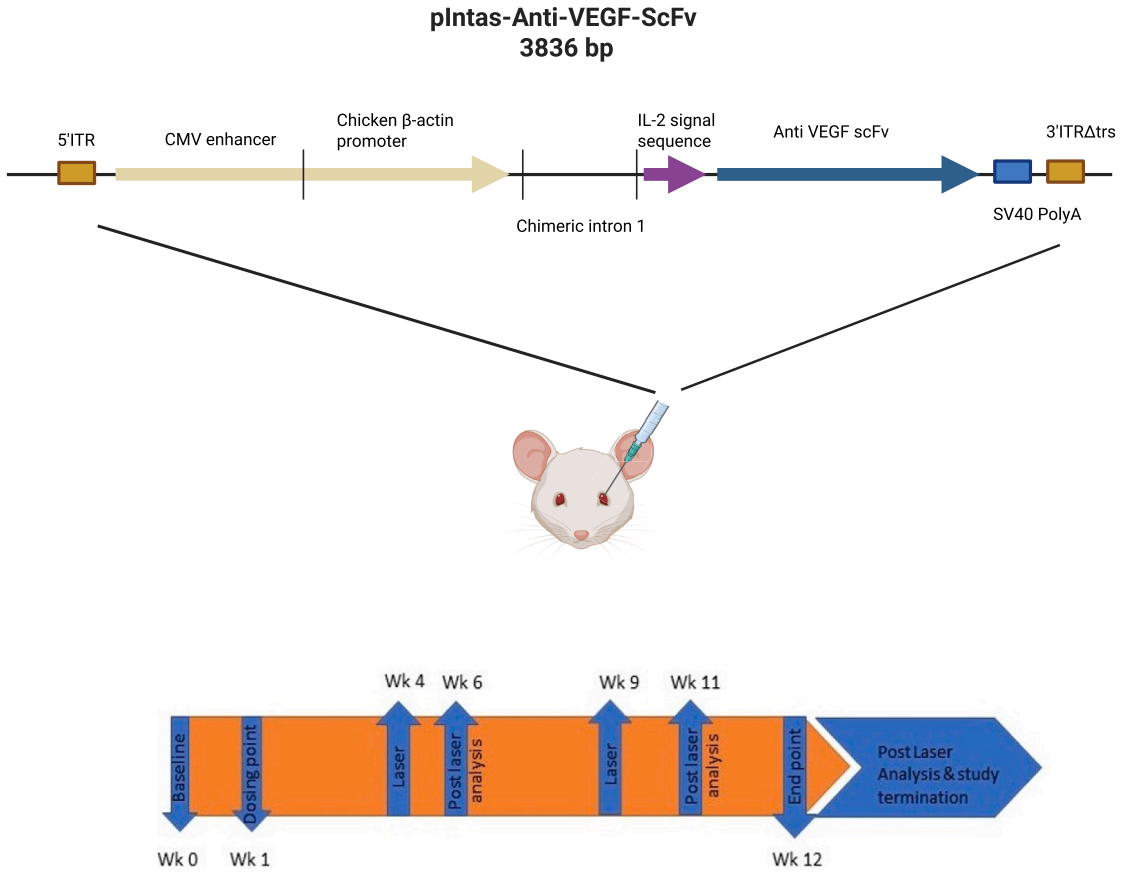

Figure 1. Anti-VEGF scFv expression cassette and *in vivo* study design

(Top) Schematic map of the AAV plasmid (pIntas-Anti-VEGF-scFv, 3,836 bp) used to generate rAAV vectors encoding a secreted anti-VEGF single-chain variable fragment (scFv). The expression cassette comprises a CMV enhancer/chicken β-actin promoter (yellow), chimeric intron, IL-2 signal sequence (purple), anti-VEGF scFv (navy blue), and SV40 poly(A) (blue), flanked by AAV 5′ and 3′ ITRs (orange). Bacterial propagation elements (origin of replication and kanamycin resistance) are indicated (green and pink, respectively). (Bottom) Study timeline showing baseline assessments were performed at week 0, followed by subretinal dosing at week 1. Laser CNV induction was performed at weeks 4 and 9, with post-laser analyses at weeks 6 and 11, respectively. Animals reached endpoint at week 12, when post-laser analysis and study termination procedures were completed.

other anti-VEGF drugs available at the time. It is a small molecular size scFv with the absence of an Fc portion, allowing for higher molar concentration to be injected into the intravitreal cavity.[23,24] Results in nonhuman primates revealed its high efficacy, low systemic exposure, and no toxicity,[25] showing its potential as a potent anti-VEGF treatment for nAMD. However, early reports from phase 3 clinical trials revealed the occurrence of an emerging side effect of retinal vasculitis.[26,27] As a result, safety concerns have been raised which halted the use of brolucizumab worldwide. In this proof-of-principle study, we assessed the efficacy of an AAV-based gene therapy delivering expression of humanized anti-VEGF scFv (Intas Pharmaceutical Ltd, Ahmedabad, India) similar to brolucizumab, packaged in two different adeno-associated viruses (rAAV6 and 8), for exploring the efficacy of photoreceptors and RPE transduction, as a gene therapy treatment in a laser-induced CNV mouse model. We report two novel observations, (1) treatment with an AAV-based gene therapy product, inhibits CNV in a laser-induced mouse model, and (2) prolonged suppression of CNV can be achieved by AAV-delivered scFv.

RESULTS

rAAV treatment with anti-VEGF inhibits blood vessel leakage in a laser induced CNV mouse model

The humanized monoclonal scFv that binds and inhibits VEGF was packaged into two different rAAV serotypes, rAAV6 and rAAV8, both of which are known for their specificity in targeting the photoreceptors and RPE,[28–31] and injected via transscleral subretinal delivery in three doses (1.00E+09 VG/eye [low], 3.00E+9 VG/eye [medium], and 1.00E+10 VG/eye [high]) (Figure 1). A total of 79 mice were observed, creating 556 spots across the two time points (Figure 2A). The groups comprised rAAV6/8 low, medium, and high doses, a control (no vector/no treatment in either eye), or a placebo (phosphate buffer saline (PBS) with 0.001% w/v Pluronic F-68) in right eye only. Prior to treatment (week 0) with the humanized

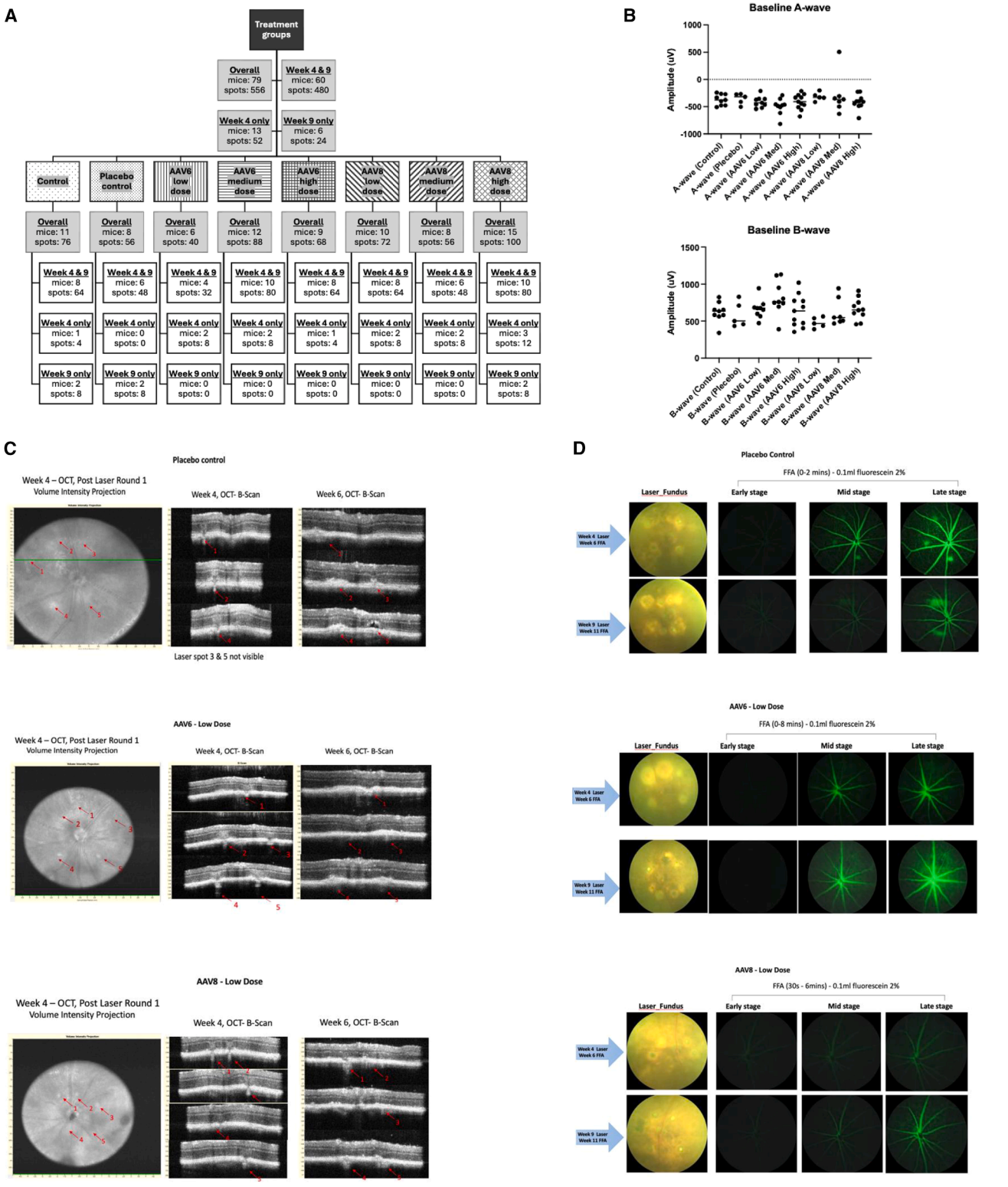

(legend on next page)

monoclonal scFv against VEGF, the visual function and retinal structure of mice were examined by electroretinogram (ERG) (Figure 2B) and color fundus photography (CFP) combined with optical coherence tomography (OCT) (data not shown). ERG measures the electrical activity of the light sensitive cells (rods and cones) in the retina in response to light stimulus. Baseline ERGs describe pre-intervention photoreceptor function and provide a reference for post-treatment comparison. The amplitudes from baseline to the A-wave was on average around 400 μV across all groups, while those in the B-wave peak varied around 500 μV. CNV was performed in week 4 and week 9 by applying four retinal lesions circumferentially to encircle an area of the optic disc, which was confirmed by fundus imaging and OCT (Figure 2C; Figure S1A). To avoid interference in CNV creation, the second laser spots were applied near but not on the previous spots. The effects of laser treatment to the retina were evaluated by fundus fluorescein angiography (FFA) to confirm and quantify the CNV lesion size and to determine leakage, OCT was then carried out to assess retinal damage. For the control groups, OCT scans showed leakage and increased scarring at the laser spots, whereas for the AAV-treated groups (AAV6 and AAV8), we observed no or minimal leakage with scarring still visible but merely healing at point of laser (Figure 2C). To determine the efficacy of the AAV anti-VEGF treatment, FFA were analyzed for presence or absence of blood vessel leakage at week 6 or 11 of the experiment and expressed as a binary measure (Yes/No) and summarized with frequencies and percentages. Leakage was graded by comparing the diameter of the bleeding area with the lesion diameter. Lesions with hemorrhage smaller than the lesion were used for statistical analyses.[32] Each laser spot was treated as an independent experiment, so the presence or absence of leakage was determined out of a maximum of five laser spots at each time point. Leakage was evaluated by reviewing both OCT images and also fundus fluorescein angiograms (Figure 2D), the disappearance of laser spots were evident in fluorescein images, occasionally, no laser spots were observed.

rAAVs packaging anti-VEGF scFv achieve sustained expression in the retina and did not result in a dramatic immune response

To examine the sustained expression of the anti-VEGF scFv rAAV vectors in the retinae of the treated mice, quantitative polymerase chain reaction (qPCR) analysis was performed twelve weeks after subretinal injections (Figure 3A), showing dose escalation response reflecting the viral vector dose, where fold change in the vector copies ranged between 1.126 to 2.028 and 1.362 to 1.513 for the rAAV6 and rAAV8-treated groups, respectively. Notably, the rAAV8 low dose showed a higher fold change (2.129) than the medium and high dose-treated groups. To evaluate if the vector transcripts were translated into protein, we examined the expression of a scFv against VEGF with immunohistochemistry analysis. The expression in the photoreceptor layer was more robustly seen in the AAV-6-treated eyes than that of the AAV8 treated (Figure S2), suggesting better transduction of the photoreceptor layer achieved with the rAAV6 serotype. Protein-level quantification (e.g., ELISA or immunoblot) was not performed; therefore, immunohistochemistry should be interpreted as semi-quantitative. Next, we evaluated the effect of the drug/placebo on retinal function after treatment by performing ERG analysis at week 12 after treatment (Figure 3B; Tables 1 and 2). We did not observe a significant change in the photoreceptors' response to light stimulus after anti-VEGF scFv AAV treatment (median amplitude values of A-waves range between −265.50 and −368.25 μV and B-waves between 409.4 and 570.1 μV), suggesting the anti-VEGF rAAV vectors did not raise safety concerns. Based on the fundus imaging and OCT of treated groups (Figure 2C; Figure S1A), scarring and disruption of the RPE/choroid was only observed in the laser spots with no obvious thinning of the retina. We occasionally observed mild signs of vitreous inflammation in OCT scans and retinal vasculitis on fluorescein angiography (with both serotypes) that we didn't see in the control groups (Figure S2).

AAV-based gene therapy treatment with anti-VEGF scFv inhibits murine CNV with sustained suppression at 4 and 9 weeks post-treatment

We evaluated the efficacy of rAAV anti-VEGF scFv at weeks 4 and 9 post-treatment following laser-induced neovascularization by assessing blood vessel leakage at laser spot sites. Here, "sustained" refers to maintenance of the inhibitory effect at both 4 and 9 weeks after vector administration. Each laser spot is considered an individual treatment, and lesions were graded for leakage, and only lesions with hemorrhage smaller than the lesion diameter were included for analysis. We counted the number of spots with and without leakage among all mice per time point, and we observed an overall decrease in the number of leakage spots in the treated groups, both with rAAV6 (week 4: 21.6% [19/88]; week 9: 26.1% [23/88]) and rAAV8 (week 4: 12.4% [12/97]; week 9: 10.4% [10/96]), compared to the controls (62.5% [20/32] at week 4 and 71.9% [23/32] at week 9) (Table 1).

Figure 2. Assessment of anti-VEGF AAV treatment in CNV-induced mice

(A) Flow diagram of leakage observations by treatment and time point. Four laser spots were used per mouse per time point (week 4 and week 9, with ERG and fundus photography and OCT performed at week 0 and subretinal injections at week 1). Sixty mice were observed at both week 4 and 9 creating 480 spots (240 at week 4 and 240 at week 9); 13 mice (52 spots) were observed at week 4 only, and 6 mice (24 spots) were observed at week 9 only. (B) Median values of baseline ERG recordings of C57BL6J mice at week 0 prior to subretinal injections of AAV6 and AAV8 anti-VEGF scFv vectors showing normal A-waves and B-waves. Baseline ERGs are shown to document pre-injection retinal function and to contextualize the 12-weeks ERG safety assessment. (C) Representative OCT scans of mice injected with anti-VEFG scFv AAV6, AAV8 low dose (1.00E + 09) VG/eye), and PBS-injected controls, red arrows represent the laser spots. (D) Representative color fluorescein angiographs (CFA) of mice with choroidal neovascularization (CNV) induced at week 4 and week 9. Images from mice injected with anti-VEFG scFv AAV6 (low dose), AAV8 (low dose), and PBS-injected controls. For placebo control, medium and high doses of AAV6 and AAV8-treated groups (see Figure S1). Color fundus photographs used to visualize the laser spots at each time point, CFA was used to determine blood vessel leakage at early (30 s), medium (4 min), and late stages (8 min) after fluorescein injection.

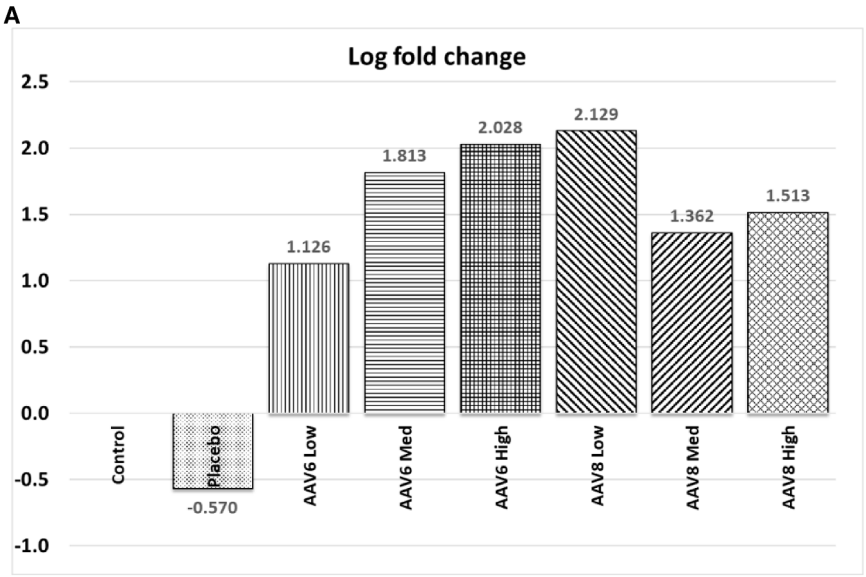

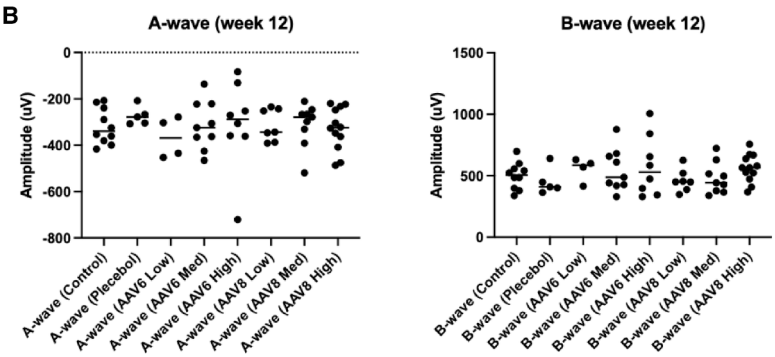

Figure 3. Anti-VEGF scFv AAV expression profile following treatment

(A) Quantitative polymerase chain reaction (qPCR) analysis showing transcript levels of neural retina of the AAV6 and AAV8 anti-VEGF scFv vectors at week 12 after AAV treatment. The log fold changes shown are from averaged ct values of (n = 2 to 3) per group. (B) Median values of ERG recordings per treatment group at week 12 following AAV treatment with anti-VEGF scFv AAVs showing no significant change in A-waves and B-waves, to compare the changes in the mice between week 0 and week 12 for the B wave and for A wave (continuous data) per treatment group, paired sample t tests were performed as the distribution of the differences between the two time points were normal. Mean and SD were presented to summarize these data per treatment group, time point and wave type. Statistical significance was reached when $p < 0.001$ due to multiple testings performed

In contrast, we observed a noticeable increase in the percentages of "no leakage" spots in both week 4 and week 9 treatment groups compared to the controls (Table 2; Figure 4). In particular, we observed a significant dose-dependent increase in the percentage of "no leakage" spots in the rAAV6-treatment group at week 9 time point (56.3%, 62.5%, and 96.9% for the low, medium, and high doses, respectively, Table 1). Similarly, in the rAAV8-treated group, the increase was similar among the doses (87.5%, 91.7%, and 90.0% for the low, medium, and high doses, respectively, Table 1) compared to the control (28.1% and 25.0% for the PBS-treated and placebo controls, respectively).

Next, we performed immunohistochemistry analysis on whole-mount retinae from rAAV6 and rAAV8 anti-VEGF scFv-treated and control groups to assess the area (in μm^2) of new blood vessel formation (Figure 5A). With the highly positively skewed data, the medians with lower quartiles (LQ) and upper quartiles (UQ) were presented in boxplots (Figure 5B) with summary statistics of area stained for new blood vessels from each laser spot by treatment groups (Table S1), assuming the laser spots were independent of each other. Comparisons of area stained for new blood vessels from each laser spot between treatment groups (Table 3) further demonstrates the reduction in CNV spots. The median from each group represents the 50th percentile (midpoint) of the ranked data while LQ and UQ represent the 25th and 75th percentiles of the ranked data within the group. CNVs were visualized on flatmounts using confocal microscopy following lectin staining (Alexa Fluor 488), which binds specifically to endothelial cells, and quantification of neovascular area showed a significant reduction in the rAAV6- and rAAV8-treated groups compared to controls, with no clear indication of dose dependency, further supporting inhibition of murine retinal neovascularization in treated mice.

DISCUSSION

Here, we show that AAV-based gene therapy treatment of a humanized monoclonal scFv that binds and inhibits VEGFA (similar to brolucizumab), packaged in two different recombinant adeno-associated virus serotypes (rAAV6 and rAAV8) (Intas Pharmaceutical Ltd, Ahmedababd, India), which were delivered independently via subretinal injections and provided an efficacious, and relatively safe, treatment of nAMD in a laser-induced CNV mouse model. Moreover, anti-VEGF gene therapy inhibits murine CNV with a prolonged suppression effect. Treatment effects were dose dependent (with rAAV6), incremented by time point, and targeted to laser-induced spots. The dose-dependent response was evident with rAAV8 with the low and medium dose, except for the high dose, where the pattern was disrupted, possibly due a vector related toxic effect.

Table 1. Leakage status by treatment groups at week 4 and 9

			AAV6			AAV8		
Leakage	control	placebo control	low dose	medium dose	high dose	low dose	medium dose	high dose
At week 4								
No	12 (37.5%)	13 (54.2%)	12 (75.0%)	30 (75.0%)	27 (84.4%)	29 (90.6%)	23 (95.8%)	32 (80.0%)
Yes	20 (62.5%)	11 (45.8%)	4 (25.0%)	10 (25.0%)	5 (15.6%)	3 (9.4%)	1 (4.2%)	8 (20.0%)
At week 9								
No	9 (28.1%)	6 (25.0%)	9 (56.3%)	25 (62.5%)	31 (96.9%)	28 (87.5%)	22 (91.7%)	36 (90.0%)
Yes	23 (71.9%)	18 (75.0%)	7 (43.8%)	15 (37.5%)	1 (3.1%)	4 (12.5%)	2 (8.3%)	4 (10.0%)

Limited to mice that were observed at both time points (mice = 60, spots = 240[a] at week 4 and 240[a] at week 9). Results presented are showing the number and percentage of laser spots within group.
[a]Four laser spots were used for each mouse.

The hallmark feature of nAMD is the presence of CNVs, which are neovascular structures in the choroid mediated by VEGF,[11,33] along with fluid exudation and subretinal fibrosis.[5] Therapeutic strategies for nAMD transitioned from laser therapy that ablates the lesions to using an anti-VEGF approach to target the pathology directly. There is an increasing awareness that anti-VEGF agents are favorable prognosis tools for nAMD; however, they are associated with substantial financial burdens, as well as the need for frequent administration. Emerging therapies aim to extend the intervals between treatments and provide efficacious treatments.

The efficacy of anti-VEGF treatment was assessed by observing the leakage status (presence or absence of blood vessel leakage) at the laser spots used to induce CNV, each laser spot was treated as an independent treatment, so the presence or absence of leakage was determined by reviewing OCT scans (when possible) and fundus fluorescein angiograms. The laser spots were applied at two time points to assess the sustainability of the gene therapy treatment since laser CNV spontaneously regress overtime,[34–36] which is a drawback with CNV models, and the two-stage laser model has been developed to combat this.[37] Hence, the second CNV induction provided evidence for sustainable inhibition of VEGF. The effect of CNV inhibition was dose-dependent with the rAAV6 cohort with the percentage of "no leakage" status increased in the treatment groups, at week 4 and week 9 of the experiment, compared to the controls. This observation further elucidates the efficacy of the anti-VEGF treatment, which agrees with previous studies of anti-VEGF treatment agents in nAMD models including rhesus monkeys, guinea pigs, rats, and mice.[13,38–42] Two weeks (14 days) after CNV induction is a widely accepted time point to analyze the treatment effect.[32,43,44] While CNV lesions reach their peak size around 7 to 10 days post-laser, they generally stabilize or remain consistent between 7 and 14 days, providing a stable, mature, and measurable lesion for evaluation.

Recent anti-VEGF gene therapy with AAV dual-acting vector, RNAi, AAV-multiple gene therapy combining VEGF-targeting miR-RNAs, and adenovirus-mediated multiple gene approaches[45–48] further elucidates the potential therapeutic implication of VEGF inhibition. Performing summary statistics on flat-mount retinae of area stained for new blood vessels (μm^2) from each laser spot by treatment groups revealed an overall decrease in new blood vessel formation in the treated eyes compared to the control. This observation further supports the assumption that this AAV-based gene therapy approach is likely to be efficacious and of clinical relevance, since studies have demonstrated that anti-VEGF therapies lead to a decrease in choroidal thickness and vascularity, indicating a reduction in neovascularization.[49] Additionally, research has shown that CNV subsides following anti-VEGF drug treatment (reviewed in Cheng et al.[50]), further supporting the therapy's efficacy in inhibiting abnormal blood vessel growth associated with nAMD.

Currently, approved anti-VEGF agents including ranibizumab, aflibercept, and brolucizumab are used to manage nAMD (reviewed in ElSheikh et al.[51]). However, the repeat rate of treatment intervals with most of these drugs represents a drawback for patients' care. In contrast, due to the small molecular weight of brolucizumab, which is a scFv in contrast to double chain antibodies with Fc portion, it allows for a higher molar concentration to be injected into the intravitreal cavity.[23] An scFv is an autonomous binding agent that is no longer dependent on a heavy molecular support structure for potent target binding.[52,53] Although the early-real-world visual outcome of the use of brolucizumab did not flag safety flags,[54] concerns have been raised due to the incident of intraocular inflammation (IOI),[55] with patients developing retinal vasculitis and/or retinal vascular occlusion. The AAV-based gene therapy treatment with the newly formulate anti-VEGF scFv presented in this study did not show obvious safety concerns. Observation of OCT scans at the laser induction (week 4) and the analysis (week 6) time points reveal no obvious leakage, only scarring with merely healing signs at the point of laser spots, which is expected. This observation indicates quiescence/fibrotic state of the CNVs and an encouraging sign of the safety aspect of the treatment. It is difficult to comment on long term damage from scarring/fibrosis without staining with the appropriate markers such as collagen or fibronectin.

Effective gene therapy relies on the efficient delivery of therapeutic agents to target cells/organs. Viral vectors are engineered to retain

Table 2. Comparison of no leakage spots between treatment groups at week 4 and 9

	At week 4		At week 9	
Comparison of no leakage	difference (95% CI)	P[a]	difference (95% CI)	p[a]
Placebo control – Control	16.7% (−9.1%, 39.8%)	0.214	−3.1% (−24.7%, 20.4%)	0.794
AAV6 low dose – Control	37.5% (7.5%, 58.3%)	0.014	28.1% (−0.7%, 52.3%)	0.058
AAV6 medium dose – Control	37.5% (14.5%, 55.6%)	0.001	34.4% (11.2%, 52.7%)	0.004
AAV6 high dose – Control	46.9% (23.3%, 63.9%)	<0.001	68.8% (47.4%, 81.6%)	<0.001
AAV8 low dose – Control	53.1% (30.4%, 68.9%)	<0.001	59.4% (36.1%, 74.0%)	<0.001
AAV8 medium dose – Control	58.3% (34.8%, 73.3%)	<0.001	63.5% (39.0%, 77.5%)	<0.001
AAV8 high dose – Control	42.5% (19.8%, 59.9%)	<0.001	61.9% (40.2%, 75.8%)	<0.001
AAV6 low dose – Placebo control	20.8% (−9.5%, 45.0%)	0.182	31.3% (0.8%, 55.7%)	0.046
AAV6 medium dose – Placebo control	20.8% (−2.7%, 42.8%)	0.086	37.5% (12.3%, 56.1%)	0.004
AAV6 high dose – Placebo control	30.2% (6.1%, 51.2%)	0.013	71.9% (48.3%, 85.1%)	<0.001
AAV8 low dose – Placebo control	36.5% (13.2%, 56.5%)	0.002	62.5% (37.2%, 77.5%)	<0.001
AAV8 medium dose – Placebo control	41.7% (17.6%, 61.1%)	<0.001	66.7% (40.2%, 81.0%)	<0.001
AAV8 high dose – Placebo control	25.8% (2.6%, 47.2%)	0.029	65.0% (41.2%, 79.3%)	<0.001

Results presented representing difference in percentage of spots had no leakage, assuming each laser spot was independent of each other. Limited to mice that were observed at both time points.

Chi-square tests were performed to assess the assocation between leakage status and treatment groups (each AAV6/AAV8 group vs. Control/Placebo control group). Differences of no leakage between the two treatment groups were presented with 95% CI and *p* value.

[a]Chi-square tests were performed.

high transduction efficiency and stable gene expression.[56] Overall, both rAAV6 and rAAV8 anti-VEGF scFv vectors showed sustained and dose-dependent responses in the treated retina of all treated groups, the increase in fold change in the rAAV8 low dose can be explained by a possible toxic effect of the medium and high dose of the rAAV8 vector. The fold change in the DNA transcripts in the medium and low dose of the rAAV8-treated group is remarkably lower than those of the rAAV6-treated group, which shows a dose dependant response, suggesting a dose toxicity effect might have contributed to this observation, although no obvious toxicity signs were noticed in the OCT scans, similarly, no noticeable functional deficits were seen in the ERG recordings of both the rAAV-6 and the rAAV8-treated groups. As far as the expression of the rAAV vectors packaging the scFv against VEGF, both serotypes seem to be expressed by the photoreceptor layer of the treated mice, judged by immunohistochemistry analysis of stained retinae with anti-scFv antibodies, suggesting a potent delivery of the rAAV vectors. Both serotypes have been shown to be specific to the photoreceptors and RPE, respectively,[28,30,57] so our observations agree with those reported in the literature.

The limitation of the study lies in its relative complexity. Clinically, the incidence of "vasculitis" with brolucizumab is about 1:10,000 so this study cannot address the incidence or effects of this side effect. Scientifically, the outcomes were measured using a variety of techniques such as immunohistochemistry, and qPCR which meant certain compromises needed to be made to satisfy the need for tissue processing. It would also have been simpler not to re-laser the mice and measure the leakage status at a later time point only. Despite these limitations, several novel observations were made. Firstly, AAV gene therapy treatment with the newly formulated anti-VEGF scFv (similar to brolucizumab) inhibits murine CNV . Secondly, prolonged suppression of CNV can be achieved by this AAV-based gene therapy approach. Both rAAV6 and rAAV8 serotypes were efficacious in transducing the photoreceptors in the retina. Mild signs of inflammation (uveitis/vasculitis) were occasionally seen with both serotypes, which is of significant clinical relevance. This could be for a variety of reasons. Human clinical trials with AAV vectors would need to be done initially with a low concentration of vector prior to dose escalation. It may be prudent to assess for toxicity on another model prior to clinical trials. Although mouse models of CNV may not predict human immune mediated retinal vasculitis, and that the results shown in this study do not establish reduced immunogenicity relative to brolucizumab. In addition, it was difficult to predict the immunogenicity of the scFv since the placebo control was a saline only, not a non-expressing scFv, so any safety conclusions are based on the CNV model rather than transgene-specific immune comparisons, and that any comparison in this proof-of concept study is conceptual (sustained expression to reduce treatment frequency) rather than a definitive head-to-head clinical efficacy claim. However, the results suggest any future applications in humans would be best done initially with a low concentration of vector prior to dose escalation, and while the data in this study support efficacy in a mouse CNV model, direct comparisons to brolucizumab would require matched dosing, timing. In addition, it may be prudent to assess for toxicity in another animal model, such as nonhuman primate, prior to human clinical trials.

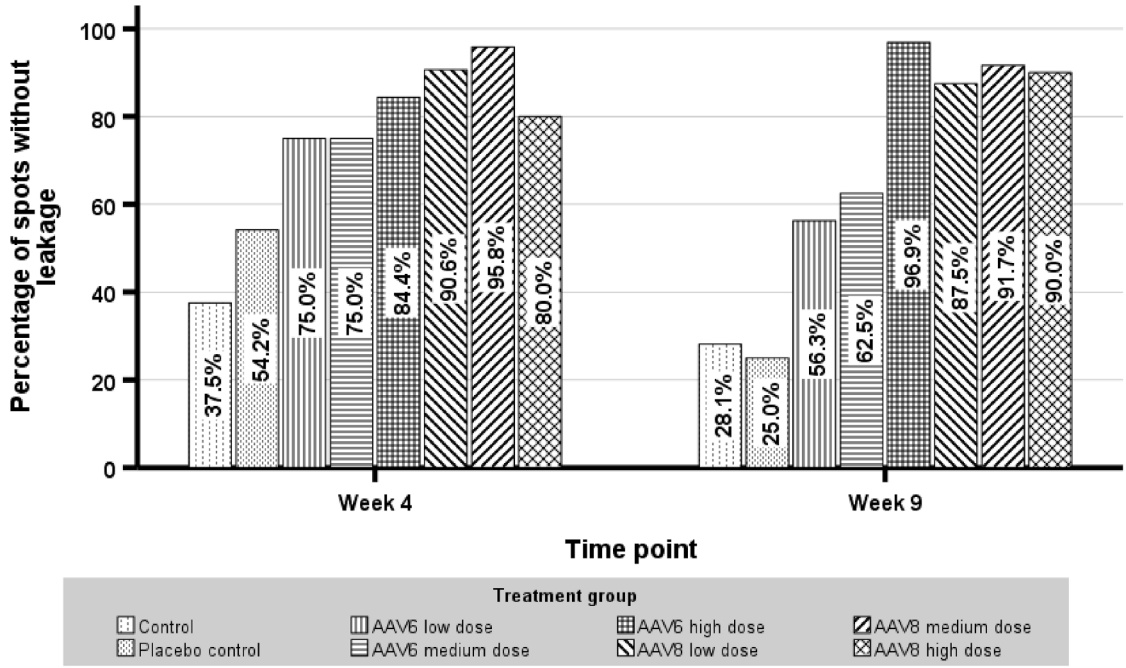

	Week 4, mice n= 73	Week 9, mice n= 66
Total number of laser spots fired	292	264
Laser spots with No leakage	219	73
Laser spots with leakage	178	86

Figure 4. Assessment of leakage status after anti-VEGF AAV treatment

Percentage of laser spots without leakage by treatment group at week 4 and at week 9 (mice = 60, spots = 240 at week 4 & 240 at week 9). Limited to mice that were observed at both time points. Leakage status (based on fluorescein angiographs) from each laser spot was expressed as a binary measure (Yes/No) and summarized with frequencies and percentages within treatment group at week 4 and at week 9. Chi-square tests were performed to assess the association between leakage status and treatment groups (each AAV6/AAV8 group vs. control/placebo control group). Differences of no leakage between the two treatment groups were presented with 95% CI and *p* value.

MATERIALS AND METHODS

AAV production

Recombinant AAV6 and AAV8 full particles expressing anti-VEGF scFv were produced in a wave bioreactor in batch mode, using the triple-transfection method in HEK293 cells. The transgene plasmid pIntas-Anti-VEGF-ScFv, the AAV helper plasmid containing *Rep* and *Cap* genes, and the adenoviral helper plasmid were co-transfected into HEK293 cells at a plasmid ratio of 1:1.5:2, respectively. Cultures were harvested 72 h post-transfection. The harvested cultures were then subjected to chemical lysis followed by benzonase treatment prior to clarification. The harvested culture was clarified using DOSP depth filter. The depth-filtered lysate was further clarified through sequential filtration using 0.45 and 0.22 μm filter. The clarified harvest was purified using an affinity capture step with Poros CaptureSelect AAVX resin. Post-capture, the product was buffer exchanged and concentrated using 100 kDa UFDF cassettes. Following UFDF, the material was further purified by density-based ultracentrifugation for separation of filled and empty AAV capsids. The ultracentrifuged fraction was subsequently processed through a Sartobind Q membrane to remove any residual process-related impurities. Finally, the product was buffer exchanged into PBS using 100 kDa Amicon, and the drug substance (DS) was prepared.

Animal housing and husbandry

All experimental procedures were approved by a local ethical review committee and conducted in accordance with personal and project licenses (PP9872126) under the UK Animals (Scientific Procedures) Act (1986). Experiments were conformed to the ARVO statement for the Use of Animals in Ophthalmic and Vision Research (Annexure 1). 8–10 weeks C57BL/6 female mice were bred and maintained at

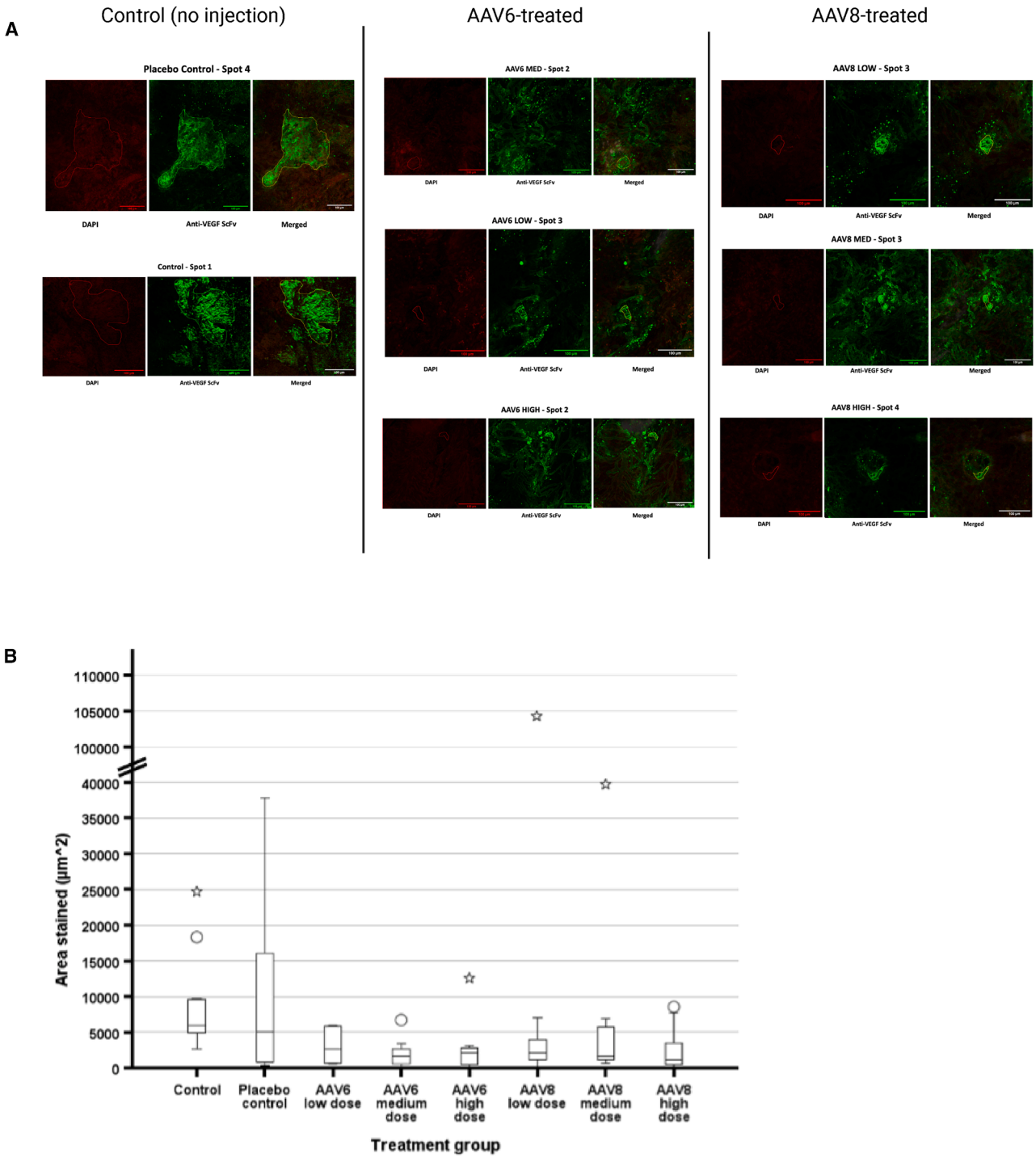

Figure 5. Choroidal neovascularization measurement

(A) Representative images of wholemount retinae injected with PBS-control, AAV6, and AAV8 anti-VEGF scFv vectors showing measurements of the area of choroidal neovascularization (CNV), judged by staining with Alexa Fluor 488-labeled lectin stain (1:100) (green), using FiJi ImageJ software. A hands-free tool was used to draw around the CNV area (yellow). DAPI was used as a nuclear counterstain (pseudo colored red). Each selection was saved in the region of interest (ROI) manager and all areas were measured. The measurement was performed by two independent blinded investigators. An average of each measurement was taken. (B) Box and whisker plots of area stained for new blood vessels (μm^2) between treatment groups, with the line at the center of box represents median, bottom and top of the box represent lower and upper quartiles respectively. Circle and star indicating outlier and extreme values respectively.

Table 3. Comparisons of area stained for new blood vessels (μm²) from each laser spot between treatment groups, assuming each laser spot was independent of each other

Comparison of area stained	median difference (95% CI)[a]	P[b]
Placebo control – Control	2166.8 (−4596.5, 5452.6)	0.443
AAV6 low dose – Control	3619.1 (50.0, 9002.6)	0.037
AAV6 medium dose – Control	4791.2 (2903.3, 7371.3)	<0.001
AAV6 high dose – Control	4420.6 (2108.5, 8903.9)	0.007
AAV8 low dose – Control	3884.9 (1704.9, 6456.0)	0.006
AAV8 medium dose – Control	4061.3 (1049.6, 6562.5)	0.021
AAV8 high dose – Control	4977.1 (2884, 7070.9)	<0.001
AAV6 low dose – Placebo control	1068.9 (−2122.5, 17048.2)	0.646
AAV6 medium dose – Placebo control	3054.7 (−445.3, 10262.1)	0.104
AAV6 high dose – Placebo control	2567.9 (−1525.8, 18502.7)	0.227
AAV8 low dose – Placebo control	1078.3 (−1628.1, 8875.3)	0.449
AAV8 medium dose – Placebo control	634.1 (−1299.1, 9249.1)	0.674
AAV8 high dose – Placebo control	2827.0 (2.4, 9870.0)	0.048

[a]95% CI and *p* values were calculated with equal variances not assumed (due to SD in one group is more than double of the other comparison group).
[b]Mann-Whitney U tests were performed.

the Biomedical Research Facility (BRF) at the University of Southampton, UK. Animals were maintained in conventional cages at a constant temperature of 22 ± 2°C containing Lignocel 2/2 bedding (IPS Ltd., London, UK) and environmental enrichment on a 12/12-h light/dark cycle and were provided with food and water ad libitum. All mice were fed with a standard chow-based diet (RM1 diet; Special Diet Service [SDS] Ltd., UK) containing 7% kcal fat. All experiments were performed in the light stage of the light-dark cycle between 9:00 and 18:00 h. Mice were euthanized at experimental endpoints via a schedule 1 method.

Anesthesia for *in vivo* experiments

Mice were administered reversible anesthesia with a combination of ketamine (80 mg/kg, Chanelle) and xylazine (8 mg/kg, Bayer) in 0.1 mL of saline by intraperitoneal (I.P) injection using a 27G needle (BD Microlance) on a 1 mL syringe (Thermo Fisher Scientific). Mouse pupils were maximally dilated using 1% tropicamide and 2.5% phenylephrine hydrochloride eye drops (Bausch & Lomb). The corneas of mice were kept hydrated throughout treatments and imaging procedures carried out with repeated topical application of artificial tears (Viscotears, Alcone). Anesthesia was reversed at the conclusion of the procedure with 2.5% Antisedan (Centaur Services) in sterile saline at 8 μL/g of mouse weight. Animals were recovered in a warm chamber set at 37°C and then monitored for 24 h post procedure.

Full-field ERG

Mice were dark adapted for 12 h prior to ERG recordings and maintained at 27°C throughout the duration of the procedure. Anesthetic was administered and eyes were dilated. ERG traces were recorded using the Generation II Image-Guided ERG modality attachment to the Micron III Retinal Imaging System (Phoenix Research Labs, Pleasanton, CA, USA) which was housed inside a 6-panel aluminum copper mesh Faraday cage (Micro Control Instruments Ltd., Framfield, UK) to minimize potential electrical interference. Animals were placed on a heated platform and were connected to three electrodes as follows: (1) a ground electrode (inserted into the base of the tail), (2) a reference electrode that was attached to the head, and (3) an electrode with corneal contact, which was achieved by positioning the cornea onto the gold-plated objective lens. ERGs were recorded by stimulation with white LED light (6.8 cd-s/m2) of 1.5 mm diameter for 1 ms. Stimulation was performed in two sweeps with a two-minute interval from which an average recording was determined. In all cases, oculus dexter measurements were carried out first. ERGs were visualized in the V3 Phoenix LabScribe ERG software suite (Phoenix Research Labs, Pleasanton, CA, USA). A-wave and B-wave amplitudes were calculated as the measurement from baseline to the A-wave trough and the A-wave trough to the B-wave peak, respectively. The implicit time (the time interval between stimulus onset and the wave peak) for both the A and B waves was also recorded.

In vivo imaging

Anesthetic was administered and eyes were dilated. CFP were acquired with a camera and bright field imaging (450–650 nm) incorporated into the laser injector and visualized using the Phoenix Micron III Retinal Imaging Microscope Software.

Laser-induced CNV

Laser was applied to one eye of anesthetized mice with dilated pupils using a OcuLight TX Green 532 nm laser (Carlton, Buckinghamshire, UK) with a laser injector lens connected to a Micron III Retinal Imaging Microscope (Phoenix Research Labs, Pleasanton, CA, USA). The laser injector has a camera for obtaining CFP, enabling orientation and visualization of the lasered area. The retina was targeted with a focused laser beam (400 μm diameter) at a power of 800 mW for 500 ms per spot. A retinal lesion was induced with four or five laser spots, applied circumferentially to encircle an area of the optic disc at two time points (week 4 and week 9) with the second spot applied near but not on the previous laser spot. Each laser spot was treated as an independent experiment.

OCT

Anesthetic was administered and eyes were dilated. OCT imaging was undertaken using the Leica Envisu R2200 VHR SDOIS Mouse Imaging System (Leica, IL, USA). Animals were positioned on the scanning platform, we obtained 1.4 mm^3 volumetric scans (consisting of 100 B-scans and 1000 A-scans per scan) using InVivoVue 2.4 Diver software (Leica Microsystems, IL, USA). Progression of laser-induced retinal lesions was evaluated by the area and thickness of the point of laser induced CNV at all-time points.

Transscleral subretinal injection surgery

Transscleral subretinal injections were carried out via the choroid and Bruch's Membrane without retinal penetration using a Stativ

Opmi CS/S4 surgical microscope (Carl Zeiss Ltd., Cambridge, UK). This method is preferred over intravitreal injections as it not only delivered treatment in close proximity to the photoreceptors and RPE, the main cell types compromised in AMD, but also circumvented post-operative inflammatory complications such as vitritis and endophthalmitis. Under anesthesia, the animal's right pupil was dilated using one drop of Tropicamide 1% eye drops, blotting off after 5 min then applying one drop of phenylephrine hydrochloride 2.5% eye drops. Eye drops were blotted off and one drop of Proxycaine 2% local anesthetic was applied to the eye. Paracentesis was performed using a 33G sterile needle, by puncturing the cornea on the boundary between the iris and the ciliary body relieving pressure in the eye globe. Viscotears eye gel was applied to the eye and a 6 mm glass coverslip was placed onto the cornea to prevent light diffraction and tooth forceps were used to stabilize the globe and provide counter traction during unilateral transscleral subretinal injection. A beveled 35-gauge needle on a Nanofil syringe (World Precision Instruments, Inc) was inserted at an oblique angle through the sclera until the tip was visualized under the retina and was slowly advanced forwards parallel to the retina to create space for the subretinal injection/bleb. 1.5 μL (batch 1A) and 2 μL (batch 1B and 2) of the rAAV anti-VEGF scFv vector/placebo (see dosing dilutions table, Section 2) was slowly injected. The needle was then carefully retracted from the globe. Chloramphenicol antibiotic eye drops were applied to the eye. Success of the subretinal injection was confirmed by observing presence of a retinal bleb through the operating microscope. An anesthetic reversal (Antisedan) was administered, and animals were recovered in a warm chamber set at 37°C, then monitored for 24 h post procedure.

FFA

Effects of laser treatment to the retina and CNV lesion size measurements were evaluated by FFA, at week 6 and week 11. Images were captured via a Micron III Retinal Imaging Microscope with imaging lens (Phoenix Research Labs, Pleasanton, CA, USA) using a blue filter at a wavelength of 490 nm and obtaining an image of the fluorescent green light that is emitted by the fluorescein dye. While under reversible anesthesia, mouse pupils were maximally dilated using 1% tropicamide and 2.5% phenylephrine hydrochloride eye drops (Bausch & Lomb). The corneas of mice were kept hydrated throughout treatment and imaging procedures carried out with repeated topical application of artificial tears (Viscotears, Alcone). 2% fluorescein (Bausch & Lomb) was administered by IP injections maximum dose 0.1 mL/mouse. Images were acquired with Micron lll imaging software at intervals of 30 s up to 8 min. Mice were recovered by administration of Antisedan up to 0.2 mL/mouse and given up to 1 mL of saline for hydration via IP injection. Animals were recovered in a warm chamber set at 37°C and then monitored for 24 h post procedure.

Eye tissue collection—Immunohistochemistry

Eyes were enucleated at week 12 and stored in a 2 mL tube in 4% paraformaldehyde (PFA) for 2 h at 4°C. Eyes were then transferred to a fresh tube with PBS and stored at 4°C ready for processing. For immunohistochemistry the cornea and lens were dissected under a microscope (Leica EZ4) and eye cups (Sclera-RPE choroid and neural retina) were cryoprotected in a series of sucrose (5%–10%) and imbedded in optimal cutting temperature compound (OCT). 16 μm cryo sections were permeabilized in PBST (PBS 0.3% Triton) with 1% bovine serum albumin for 5 min then blocked in 5% goat serum in PBST for 45 min before incubation with primary antibodies (FITC-conjugated rabbit anti-scFv antibody (SS-Ab-ScFv-01-F - Intas Pharmaceuticals Ltd, Ahmadabad, India) diluted 1:2,000-fold in 1% BSA in PBST overnight at 4°C. Secondary antibodies (gout anti-rabbit IgG 555, 1:500) were applied for 2 h in the dark before mounting in Mowiol solution. For whole-mount staining, eyes were inoculated and fixed in 2% PFA for 2 h and eye cups (Sclera-RPE choroid) were radially cut to give equidistant petals converging at the optic nerve. The eye cups were washed in PBST (0.3% Tween) and then blocked with 15% goat serum in PBST (0.3% Tween) for 1 h and incubated overnight with 1:100 of lectin (2B Scientific) diluted in PBST (0.3% Tween). The following day eye cups were washed in PBST (0.3% Tween) for five minutes and stained with DAPI (1:1000) diluted in PBS for 6 min. The tissue was gently transferred to an adhesion slide with the sclera facing down and the choroid facing up. 100 μL of Mowiol was added to the slide and covered with a coverslip. Tissue was allowed to dry at 4°C in the fridge overnight and then was imaged on an SP8 Leica confocal microscope.

Eye tissue collection and processing: qPCR

Eyes were enucleated at week 12 and stored in a 2 mL tube in saline solution at 4°C. Eyes were dissected and the retina was isolated. DNA was extracted from the retina using Gen Elute Mammalian DNA Miniprep kit (Sigma Aldrich), Annexure 3. DNA samples were then used for qPCR analysis using TaqMan probes against VEGF, amplifications visualized with QuantStudio 5 system (Applied Biosystems). Mean Ct values were normalized to house-keeping gene (beta actin).

The analytical protocols used in the study

CNV measurement

Lectin stain (labeled with Alexa Fluor 488 dye, 1:100 2B Scientific) was used to visualize CNV areas in flatmounts 12 weeks after treatment. The area of CNV was measured using FiJi ImageJ software. Tiff images from the LasX software were imported into Fiji ImageJ and corrected the scale using the metadata file. A hands-free tool was used to draw around the CNV area. Each selection was saved in the region of interest (ROI) manager and all areas were measured. The measurement was performed by two independent blinded investigators. An average of each measurement was taken.

Analysis of laser-induced CNV

Retinal images were analyzed for presence or absence of leakage at week 6 or 11. Each laser spot was treated as an independent experiment, so the presence or absence of leakage was determined out of a maximal of 4 laser spots per eye at each time point. Strict exclusion criteria were followed to exclude spots that are large, confluent, or had severe hemorrhage. Laser spots were placed far enough apart

(typically 1–2-disc diameters) to prevent physical fusion. Leakage was evaluated by reviewing both OCT images and also FFA. CNVs were classified as active if both leaking on FFA and show hyperreflective lesion on OCT. The data were tabulated in an Excel spreadsheet and analyzed by a senior University of Southampton statistician.

Statistical methods

Leakage status from each laser spot was expressed as a binary measure (Yes/No) and summarized with frequencies and percentages within treatment group at week 4 and at week 9. Leakage was graded according to the diameter of the bleeding area compared to that of the lesion, if the diameter of the bleeding area less than the lesion area, these lesions were sued for statistical analyses. Chi-square tests were performed to assess the association between leakage status and treatment groups (each AAV6/AAV8 group vs. control/placebo control group). Differences of no leakage between the two treatment groups were presented with 95% confidence interval (CI) and p value. The flat-mount (new blood vessel area staining) data from each laser spot were continuous and skewed, hence were summarized with median quartile, LQ, and UQ. Mann-Whitney U tests were performed to compare the difference between treatment groups (each AAV6/AAV8 group vs. control/placebo control group) regarding the area stained for new blood vessels from the laser spots. Median difference with 95% CI and p value were presented for each comparison. For the ERG data, to compare the changes in the mice between week 0 and week 12 for the B wave and for A wave (continuous data) per treatment group, paired sample t tests were performed as the distribution of the differences between the two time points were normal. Mean and SD were presented to summarize these data per treatment group, time point, and wave type. Statistical significance was reached when $p < 0.001$ due to multiple testings performed. SPSS version 29 was used to perform all statistical analysis. Confidence interval analysis (CIA) software was used to calculate the 95% CIs for the differences between percentages.

DATA AND CODE AVAILABILITY

All data associated with this study are presented in the paper or in the supplemental information.

ACKNOWLEDGMENTS

Funding was provided by Intas Therapeutics (India). This research was also supported by the NIHR Biomedical Research Centre at Moorfields Eye Hospital and UCL Institute of Ophthalmology (United Kingdom), together with the NIHR Oxford Biomedical Research Centre (A.S. and R.E.M.).

AUTHOR CONTRIBUTIONS

A.S. and A.J.L. conceptualized the study; A.S., A.J.L., R.E.M., and H.M.Y. were involved in the study methodology; A.S., H.G., K.G., S.A.L., M.S., C.B.J., R.C.T.M., P.R., and K.M. undertook the experiments; A.J.L. and A.J.C. acquired funding; A.S. and A.J.L. supervised the project; A.S. and A.J.L. wrote the original draft; A.S., H.G., K.G., R.E.M., and A.J.L. reviewed and edited the final manuscript.

DECLARATION OF INTERESTS

The authors declare no relevant conflicts of interest.

SUPPLEMENTAL INFORMATION

Supplemental information can be found online at https://doi.org/10.1016/j.omta.2026.201756.

REFERENCES

1. Wong, W.L., Su, X., Li, X., Cheung, C.M.G., Klein, R., Cheng, C.Y., and Wong, T.Y. (2014). Global prevalence of age-related macular degeneration and disease burden projection for 2020 and 2040: a systematic review and meta-analysis. Lancet Global Health *2*, e106–e116. https://doi.org/10.1016/S2214-109X(13)70145-1.

2. Jonas, J.B., Cheung, C.M.G., and Panda-Jonas, S. (2017). Updates on the Epidemiology of Age-Related Macular Degeneration. Asia. Pac. J. Ophthalmol. *6*, 493–497. https://doi.org/10.22608/APO.2017251.

3. Joachim, N., Mitchell, P., Burlutsky, G., Kifley, A., and Wang, J.J. (2015). The Incidence and Progression of Age-Related Macular Degeneration over 15 Years: The Blue Mountains Eye Study. Ophthalmology *122*, 2482–2489. https://doi.org/10.1016/j.ophtha.2015.08.002.

4. Chou, R., Bougatsos, C., Jungbauer, R., Grusing, S., Blazina, I., Selph, S., Jonas, D.E., and Tehrani, S. (2022). Screening for Impaired Visual Acuity in Older Adults: Updated Evidence Report and Systematic Review for the US Preventive Services Task Force. JAMA *327*, 2129–2140. https://doi.org/10.1001/jama.2022.6381.

5. Ferris, F.L., 3rd, Wilkinson, C.P., Bird, A., Chakravarthy, U., Chew, E., Csaky, K., and Sadda, S.R.; Beckman Initiative for Macular Research Classification Committee (2013). Clinical classification of age-related macular degeneration. Ophthalmology *120*, 844–851. https://doi.org/10.1016/j.ophtha.2012.10.036.

6. Rispoli, M., Cennamo, G., Antonio, L.D., Lupidi, M., Parravano, M., Pellegrini, M., Veritti, D., Vujosevic, S., and Savastano, M.C. (2023). Practical guidance for imaging biomarkers in exudative age-related macular degeneration. Surv. Ophthalmol. *68*, 615–627. https://doi.org/10.1016/j.survophthal.2023.02.004.

7. Karampelas, M., Malamos, P., Petrou, P., Georgalas, I., Papaconstantinou, D., and Brouzas, D. (2020). Retinal Pigment Epithelial Detachment in Age-Related Macular Degeneration. Ophthalmol. Ther. *9*, 739–756. https://doi.org/10.1007/s40123-020-00291-5.

8. Shahidatul-Adha, M., Zunaina, E., and Aini-Amalina, M.N. (2022). Evaluation of vascular endothelial growth factor (VEGF) level in the tears and serum of age-related macular degeneration patients. Sci. Rep. *12*, 4423. https://doi.org/10.1038/s41598-022-08492-7.

9. Ferrara, N., Carver-Moore, K., Chen, H., Dowd, M., Lu, L., O'Shea, K.S., Powell-Braxton, L., Hillan, K.J., and Moore, M.W. (1996). Heterozygous embryonic lethality induced by targeted inactivation of the VEGF gene. Nature *380*, 439–442. https://doi.org/10.1038/380439a0.

10. Shirian, J.D., Shukla, P., and Singh, R.P. (2025). Exploring new horizons in neovascular age-related macular degeneration: novel mechanisms of action and future therapeutic avenues. Eye (Lond) *39*, 40–44. https://doi.org/10.1038/s41433-024-03373-x.

11. Miller, J.W., Le Couter, J., Strauss, E.C., and Ferrara, N. (2013). Vascular endothelial growth factor a in intraocular vascular disease. Ophthalmology *120*, 106–114. https://doi.org/10.1016/j.ophtha.2012.07.038.

12. Somasundaran, S., Constable, I.J., Mellough, C.B., and Carvalho, L.S. (2020). Retinal pigment epithelium and age-related macular degeneration: A review of major disease mechanisms. Clin. Exp. Ophthalmol. *48*, 1043–1056. https://doi.org/10.1111/ceo.13834.

13. Eyetech Study Group (2002). Preclinical and phase 1A clinical evaluation of an anti-VEGF pegylated aptamer (EYE001) for the treatment of exudative age-related macular degeneration. Retina *22*, 143–152. https://doi.org/10.1097/00006982-200204000-00002.

14. Eyetech Study Group (2003). Anti-vascular endothelial growth factor therapy for subfoveal choroidal neovascularization secondary to age-related macular degeneration: phase II study results. Ophthalmology *110*, 979–986. https://doi.org/10.1016/S0161-6420(03)00085-X.

15. Bakri, S.J., Thorne, J.E., Ho, A.C., Ehlers, J.P., Schoenberger, S.D., Yeh, S., and Kim, S.J. (2019). Safety and Efficacy of Anti-Vascular Endothelial Growth Factor Therapies for Neovascular Age-Related Macular Degeneration: A Report by the American Academy of Ophthalmology. Ophthalmology *126*, 55–63. https://doi.org/10.1016/j.ophtha.2018.07.028.

16. Corydon, T.J., and Bek, T. (2025). Multiple gene therapy as a tool for regulating the expression of molecules involved in neovascular age-related macular degeneration. Prog. Retin. Eye Res. *104*, 101323. https://doi.org/10.1016/j.preteyeres.2024.101323.

17. Campochiaro, P.A., Avery, R., Brown, D.M., Heier, J.S., Ho, A.C., Huddleston, S.M., Jaffe, G.J., Khanani, A.M., Pakola, S., Pieramici, D.J., et al. (2024). Gene therapy for neovascular age-related macular degeneration by subretinal delivery of RGX-314: a phase 1/2a dose-escalation study. Lancet *403*, 1563–1573. https://doi.org/10.1016/S0140-6736(24)00310-6.

18. Khanani, A.M., Aziz, A.A., Khanani, Z.A., Khan, H., Mojumder, O., Sulahria, H., Khanani, I., Khan, H., Gahn, G.M., and Mishra, K. (2025). Subretinal Gene Therapy for Treatment of Retinal and Choroidal Vascular Diseases. Am. J. Ophthalmol. *277*, 512–517. https://doi.org/10.1016/j.ajo.2024.12.002.

19. Mao, Y., Kiss, S., Boyer, J.L., Hackett, N.R., Qiu, J., Carbone, A., Mezey, J.G., Kaminsky, S.M., D'Amico, D.J., and Crystal, R.G. (2011). Persistent suppression of ocular neovascularization with intravitreal administration of AAVrh.10 coding for bevacizumab. Hum. Gene Ther. *22*, 1525–1535. https://doi.org/10.1089/hum.2011.090.

20. Cui, Y., Huo, Y., Li, Z., Qiu, Y., Yang, Q., Chen, Z., Fan, S., Huang, X., Hao, J., Kang, L., and Liang, G. (2023). VEGF-targeted scFv inhibits corneal neovascularization via STAT3 pathway in alkali burn model. Colloids Surf. *658*, 130764. https://doi.org/10.1016/j.colsurfa.2022.130764.

21. Han, N., Xu, X., Liu, Y., and Luo, G. (2023). AAV2-antiVEGFscFv gene therapy for retinal neovascularization. Mol. Ther. Methods Clin. Dev. *31*, 101145. https://doi.org/10.1016/j.omtm.2023.101145.

22. Brolucizumab (Beovu) for age-related macular degeneration (2020). Med. Lett. Drugs Ther. *62*, 23–24.

23. Sharma, A., Kumar, N., Kuppermann, B.D., Loewenstein, A., and Bandello, F. (2020). Brolucizumab: is extended VEGF suppression on the horizon? Eye (Lond) *34*, 424–426. https://doi.org/10.1038/s41433-019-0582-0.

24. Holz, F.G., Dugel, P.U., Weissgerber, G., Hamilton, R., Silva, R., Bandello, F., Larsen, M., Weichselberger, A., Wenzel, A., Schmidt, A., et al. (2016). Single-Chain Antibody Fragment VEGF Inhibitor RTH258 for Neovascular Age-Related Macular Degeneration: A Randomized Controlled Study. Ophthalmology *123*, 1080–1089. https://doi.org/10.1016/j.ophtha.2015.12.030.

25. Pignatelli, F., Niro, A., Passidomo, F., and Addabbo, G. (2021). Molecular structure, pharmacokinetics and clinical evidence of brolucizumab: a narrative review. Ann. Eye Sci. *6*, 37.

26. Dugel, P.U., Koh, A., Ogura, Y., Jaffe, G.J., Schmidt-Erfurth, U., Brown, D.M., Gomes, A.V., Warburton, J., Weichselberger, A., and Holz, F.G.; HAWK and HARRIER Study Investigators (2020). HAWK and HARRIER: Phase 3, Multicenter, Randomized, Double-Masked Trials of Brolucizumab for Neovascular Age-Related Macular Degeneration. Ophthalmology *127*, 72–84. https://doi.org/10.1016/j.ophtha.2019.04.017.

27. Kunimoto, D., Yoon, Y.H., Wykoff, C.C., Chang, A., Khurana, R.N., Maturi, R.K., Agostini, H., Souied, E., Chow, D.R., Lotery, A.J., et al. (2020). Efficacy and Safety of Abicipar in Neovascular Age-Related Macular Degeneration: 52-Week Results of Phase 3 Randomized Controlled Study. Ophthalmology *127*, 1331–1344. https://doi.org/10.1016/j.ophtha.2020.03.035.

28. Vandenberghe, L.H., Bell, P., Maguire, A.M., Cearley, C.N., Xiao, R., Calcedo, R., Wang, L., Castle, M.J., Maguire, A.C., Grant, R., et al. (2011). Dosage thresholds for AAV2 and AAV8 photoreceptor gene therapy in monkey. Sci. Transl. Med. *3*, 88ra54. https://doi.org/10.1126/scitranslmed.3002103.

29. Mussolino, C., della Corte, M., Rossi, S., Viola, F., Di Vicino, U., Marrocco, E., Neglia, S., Doria, M., Testa, F., Giovannoni, R., et al. (2011). AAV-mediated photoreceptor transduction of the pig cone-enriched retina. Gene Ther. *18*, 637–645. https://doi.org/10.1038/gt.2011.3.

30. Han, I.C., Cheng, J.L., Burnight, E.R., Ralston, C.L., Fick, J.L., Thomsen, G.J., Tovar, E.F., Russell, S.R., Sohn, E.H., Mullins, R.F., et al. (2020). Retinal Tropism and Transduction of Adeno-Associated Virus Varies by Serotype and Route of Delivery (Intravitreal, Subretinal, or Suprachoroidal) in Rats. Hum. Gene Ther. *31*, 1288–1299. https://doi.org/10.1089/hum.2020.043.

31. Suzuki, R., Katada, Y., Fujii, M., Serizawa, N., Negishi, K., and Kurihara, T. (2025). Tropism of the AAV6.2 Vector in the Murine Retina. Int. J. Mol. Sci. *26*, 1580. https://doi.org/10.3390/ijms26041580.

32. Gong, Y., Li, J., Sun, Y., Fu, Z., Liu, C.H., Evans, L., Tian, K., Saba, N., Fredrick, T., Morss, P., et al. (2015). Optimization of an Image-Guided Laser-Induced Choroidal Neovascularization Model in Mice. PLoS One *10*, e0132643. https://doi.org/10.1371/journal.pone.0132643.

33. Tan, C.S., Ngo, W.K., Chay, I.W., Ting, D.S., and Sadda, S.R. (2022). Neovascular Age-Related Macular Degeneration (nAMD): A Review of Emerging Treatment Options. Clin. Ophthalmol. *16*, 917–933. https://doi.org/10.2147/OPTH.S231913.

34. Salas, A., Badia, A., Fontrodona, L., Zapata, M., García-Arumí, J., and Duarri, A. (2023). Neovascular Progression and Retinal Dysfunction in the Laser-Induced Choroidal Neovascularization Mouse Model. Biomedicines *11*, 2445. https://doi.org/10.3390/biomedicines11092445.

35. Xie, P., Kamei, M., Suzuki, M., Matsumura, N., Nishida, K., Sakimoto, S., Sakaguchi, H., and Nishida, K. (2011). Suppression and regression of choroidal neovascularization in mice by a novel CCR2 antagonist, INCB3344. PLoS One *6*, e28933. https://doi.org/10.1371/journal.pone.0028933.

36. Iwanishi, H., Yamanaka, O., Sumioka, T., Yasuda, S., Miyajima, M., and Saika, S. (2022). Delayed regression of laser-induced choroidal neovascularization in TNFalpha-null mice. J. Cell Mol. Med. *26*, 5315–5325. https://doi.org/10.1111/jcmm.17562.

37. Little, K., Llorián-Salvador, M., Tang, M., Du, X., O'Shaughnessy, Ó., McIlwaine, G., Chen, M., and Xu, H. (2020). A Two-Stage Laser-Induced Mouse Model of Subretinal Fibrosis Secondary to Choroidal Neovascularization. Transl. Vis. Sci. Technol. *9*, 3. https://doi.org/10.1167/tvst.9.4.3.

38. Tucker, C.E., Chen, L.S., Judkins, M.B., Farmer, J.A., Gill, S.C., and Drolet, D.W. (1999). Detection and plasma pharmacokinetics of an anti-vascular endothelial growth factor oligonucleotide-aptamer (NX1838) in rhesus monkeys. J. Chromatogr. B *732*, 203–212. https://doi.org/10.1016/S0378-4347(99)00285-6.

39. Drolet, D.W., Nelson, J., Tucker, C.E., Zack, P.M., Nixon, K., Bolin, R., Judkins, M.B., Farmer, J.A., Wolf, J.L., Gill, S.C., and Bendele, R.A. (2000). Pharmacokinetics and safety of an anti-vascular endothelial growth factor aptamer (NX1838) following injection into the vitreous humor of rhesus monkeys. Pharm. Res. *17*, 1503–1510. https://doi.org/10.1023/a:1007657109012.

40. Kaiser, P.K., and Do, D.V. (2007). Ranibizumab for the treatment of neovascular AMD. Int. J. Clin. Pract. *61*, 501–509. https://doi.org/10.1111/j.1742-1241.2007.01299.x.

41. Arnold, J., Kilmartin, D., Olson, J., Neville, S., Robinson, K., Laird, A., Richmond, C., Farrow, A., McKay, S., McKechnie, R., et al. (2001). Verteporfin therapy of subfoveal choroidal neovascularization in age-related macular degeneration: Two-year results of a randomized clinical trial including lesions with occult with no classic choroidal neovascularization-verteporfin in photodynamic therapy report 2. Am. J. Ophthalmol. *131*, 541–560.

42. Grishanin, R., Vuillemenot, B., Sharma, P., Keravala, A., Greengard, J., Gelfman, C., Blumenkrantz, M., Lawrence, M., Hu, W., Kiss, S., and Gasmi, M. (2019). Preclinical Evaluation of ADVM-022, a Novel Gene Therapy Approach to Treating Wet Age-Related Macular Degeneration. Mol. Ther. *27*, 118–129. https://doi.org/10.1016/j.ymthe.2018.11.003.

43. Edelman, J.L., and Castro, M.R. (2000). Quantitative image analysis of laser-induced choroidal neovascularization in rat. Exp. Eye Res. *71*, 523–533. https://doi.org/10.1006/exer.2000.0907.

44. Giani, A., Thanos, A., Roh, M.I., Connolly, E., Trichonas, G., Kim, I., Gragoudas, E., Vavvas, D., and Miller, J.W. (2011). In vivo evaluation of laser-induced choroidal neovascularization using spectral-domain optical coherence tomography. Investig. Ophthalmol. Vis. Sci. *52*, 3880–3887. https://doi.org/10.1167/iovs.10-6266.

45. Askou, A.L., Alsing, S., Benckendorff, J.N.E., Holmgaard, A., Mikkelsen, J.G., Aagaard, L., Bek, T., and Corydon, T.J. (2019). Suppression of Choroidal Neovascularization by AAV-Based Dual-Acting Antiangiogenic Gene Therapy. Mol. Ther. Nucleic Acids *16*, 38–50. https://doi.org/10.1016/j.omtn.2019.01.012.

46. Haldrup, S.H., Fabian-Jessing, B.K., Jakobsen, T.S., Lindholm, A.B., Adsersen, R.L., Aagaard, L., Bek, T., Askou, A.L., and Corydon, T.J. (2024). Subretinal AAV delivery of RNAi-therapeutics targeting VEGFA reduces choroidal neovascularization in a

large animal model. Mol. Ther. Methods Clin. Dev. *32*, 101242. https://doi.org/10.1016/j.omtm.2024.101242.

47. Wei-Zhang, S., Cui, B., Xing, M., Liu, J., Guo, Y., He, K., Bai, T., Dong, X., Lei, Y., Zhou, W., et al. (2023). Chimpanzee adenovirus-mediated multiple gene therapy for age-related macular degeneration. iScience *26*, 107939. https://doi.org/10.1016/j.isci.2023.107939.

48. Fabian-Jessing, B.K., Askou, A.L., Jakobsen, T.S., Adsersen, R.L., Lindholm, A.B., Køllner Bjerre, A.K., Alsing, S., Bek, T., Aagaard, L., and Corydon, T.J. (2026). AAV-mediated multiple gene therapy combining VEGFA-targeting miRagshRNAs and PEDF for the suppression of choroidal neovascularization. Mol. Ther. Nucleic Acids *37*, 102833. https://doi.org/10.1016/j.omtn.2026.102833.

49. Shen, M., Zhou, H., Lu, J., Li, J., Jiang, X., Trivizki, O., Laiginhas, R., Liu, J., Zhang, Q., de Sisternes, L., et al. (2023). Choroidal Changes After Anti-VEGF Therapy in AMD Eyes With Different Types of Macular Neovascularization Using Swept-Source OCT Angiography. Investig. Ophthalmol. Vis. Sci. *64*, 16. https://doi.org/10.1167/iovs.64.13.16.

50. Cheng, S., Zhang, S., Huang, M., Liu, Y., Zou, X., Chen, X., and Zhang, Z. (2024). Treatment of neovascular age-related macular degeneration with anti-vascular endothelial growth factor drugs: progress from mechanisms to clinical applications. Front. Med. *11*, 1411278. https://doi.org/10.3389/fmed.2024.1411278.

51. ElSheikh, R.H., Chauhan, M.Z., and Sallam, A.B. (2022). Current and Novel Therapeutic Approaches for Treatment of Neovascular Age-Related Macular Degeneration. Biomolecules *12*, 1629. https://doi.org/10.3390/biom12111629.

52. Auf der Maur, A., Escher, D., and Barberis, A. (2001). Antigen-independent selection of stable intracellular single-chain antibodies. FEBS Lett. *508*, 407–412. https://doi.org/10.1016/s0014-5793(01)03101-5.

53. Thiel, M.A., Coster, D.J., Standfield, S.D., Brereton, H.M., Mavrangelos, C., Zola, H., Taylor, S., Yusim, A., and Williams, K.A. (2002). Penetration of engineered antibody fragments into the eye. Clin. Exp. Immunol. *128*, 67–74. https://doi.org/10.1046/j.1365-2249.2002.01808.x.

54. Sharma, A., Kumar, N., Parachuri, N., Sadda, S.R., Corradetti, G., Heier, J., Chin, A.T., Boyer, D., Dayani, P., Arepalli, S., and Kaiser, P. (2021). Correction: Brolucizumab-early real-world experience: BREW study. Eye (Lond) *35*, 1286. https://doi.org/10.1038/s41433-020-01351-7.

55. Saba, N.J., and Walter, S.D. (2023). Efficacy, Safety, and Durability of Brolucizumab: An 8-Month Post-Marketing Surveillance Analysis. Clin. Ophthalmol. *17*, 2791–2802. https://doi.org/10.2147/OPTH.S425709.

56. Bulcha, J.T., Wang, Y., Ma, H., Tai, P.W.L., and Gao, G. (2021). Viral vector platforms within the gene therapy landscape. Signal Transduct. Targeted Ther. *6*, 53. https://doi.org/10.1038/s41392-021-00487-6.

57. Yang, G.S., Schmidt, M., Yan, Z., Lindbloom, J.D., Harding, T.C., Donahue, B.A., Engelhardt, J.F., Kotin, R., and Davidson, B.L. (2002). Virus-mediated transduction of murine retina with adeno-associated virus: effects of viral capsid and genome size. J. Virol. *76*, 7651–7660. https://doi.org/10.1128/jvi.76.15.7651-7660.2002.